Journal of Catalysis 281 (2011) 254–262

Contents lists available at ScienceDirect

Journal of Catalysis

journal homepage: www.elsevier.com/locate/jcat

Novel catalyst structures with enhanced heat transfer characteristics

Min Sheng [a], Hongyun Yang [b], Donald R. Cahela [a], Bruce J. Tatarchuk [a,*]

[a] Center for Microfibrous Materials Manufacturing (CM^3), Department of Chemical Engineering, Auburn University, Auburn, AL 36849, USA
[b] IntraMicron Inc., 368 Industry Dr., Auburn, AL 36832, USA

ARTICLE INFO

Article history:
Received 18 January 2011
Revised 20 April 2011
Accepted 6 May 2011
Available online 11 June 2011

Keywords:
Effective thermal conductivity
Microfibrous entrapped catalyst
Packed bed
Heat transfer
Highly exothermic or highly endothermic reaction
Fischer–Tropsch synthesis

ABSTRACT

Highly exothermic and highly endothermic reactions require catalyst beds with good heat transfer characteristics. A novel catalyst structure, microfibrous entrapped catalyst (MFEC) structure, made of high thermal conductive metals can significantly improve heat transfer efficiency, compared with traditional packed beds (PB). First, the thermal parameters of metal MFEC were determined experimentally. In a stagnant gas, the radial effective thermal conductivity of Cu MFEC was 56-fold of that of alumina PB, while the inside wall heat transfer coefficient was 10 times of that of alumina PB. Compared to PB, even those made of pure copper particles, conductive metal MFEC also provides much more effective thermal conductivity and higher inside wall heat transfer coefficient in a flowing gas testing. In addition, an application of Cu MFEC in Fischer–Tropsch synthesis (FTS) demonstrated an improvement in temperature distribution inside the catalyst bed and an increase in product selectivity. Furthermore, unlike monolith catalyst structures and metallic foams, the MFEC structure is compatible with pre-manufactured catalyst particles, very flexible and ease to be corrugated. Contrast to corrugated packing with a poor conductive contribution to heat transport, MFEC with a good self-dependent thermal conductivity does not require the recycle of gas or liquid to increase the convective term of heat transfer. Therefore, the conductive metal MFEC structures serve as a great catalyst structure to enhance the intra-bed heat transfer for highly exothermic or highly endothermic reactions, reducing temperature excursions in the reactors.

1. Introduction

Because of the poor effective thermal conductivity of typical catalyst beds, heat transfer imposes a size limitation on the reactors for highly exothermic and highly endothermic heterogeneous reactions, which generate or require a large amount of heat on the surface of catalytic particles. For example, for Fischer–Tropsch synthesis (FTS), which has a reaction heat of −165 kJ/mol of CH_2 [1] and an adiabatic temperature rise of 1600 °C [2], Van Vuuren [3] summarized that the maximum diameter for tubular fixed beds with catalyst granules is 80 mm. Increasingly, endeavor to enhance heat transfer inside the reactor is made for those highly exothermic and highly endothermic reactions/processes. Generally, fluidized reactors [4,5], slurry reactors [6,7], metal monolith catalyst structures [8,9], metallic foams, and corrugated packing with open/close cross flow structure [10,11] are used to improve heat transfer efficiency inside the reactor. Though some successful applications of those methods experimentally and industrially exist, they still carry some disadvantages. For instance, the catalyst density of fluidized reactors and slurry reactors is relatively low [12]. Monolith reactor [13,14] structures and metallic foams [15] need a washcoating process to load catalytic component, which is not suitable for pre-manufactured catalysts. Corrugated packing, compatible with both washcoating and pre-manufactured catalyst particles, has been proven to have a poor conductive contribution to heat transport [16] so that a gas or liquid recycle is usually applied to improve the convective component to achieve an enhanced intra-bed heat transfer. In this paper, based on the study of thermal parameter measurements and an application in FTS process, microfibrous entrapped catalyst (MFEC), a novel enhanced heat transfer catalyst structure, is introduced to provide an alternative key to solve these problems.

The MFEC structure was developed by Auburn University and is now commercially available at IntraMicron Inc., AL. As shown in Fig. 1, MFEC is a microstructured catalyst made of sintered micron-sized metal, glass, or polymer fibers with small catalyst particles entrapped inside [17–20]. It was found that MFEC demonstrates high void volume and acceptably uniform particle distribution in the media. This high void volume significantly reduces pressure drop compared to packed beds of similar-size particles. Intra-particle mass transfer and heat transfer are enhanced due to the presence of small particles in this material versus typical extrudates used in industrial fixed bed reactors. Ultra-high contact efficiency results from using small particles entrapped in a sintered fiber matrix [21]. Several investigations have been carried out to improve the understanding of the functions of microfibrous media.

* Corresponding author. Fax: +1 334 844 2065.
E-mail address: Tatarbj@auburn.edu (B.J. Tatarchuk).

0021-9517/$ - see front matter © 2011 Elsevier Inc. All rights reserved.
doi:10.1016/j.jcat.2011.05.006

Nomenclature

C_p	heat capacity (J/kg K)
D	diameter (m)
h	inside heat transfer coefficient (W/m^2 K)
k	thermal conductivity (W/m K)
L	length of the bed
Pr	Prandtl number
r	radial position (m)
Re	Reynolds number
S	surface area (m^2)
t	time (s)
T	temperature (K)
v	superficial velocity (m/s)
V	volume (m^3)
x	mass fraction
y	volume fraction
z	axial position (m)

Greek symbols

ε	voidage
μ	gas viscosity (kg/m s)
ρ	density (kg/m^3)
φ	shape factor

Subscripts

Al	alumina
e	effective
f	fluid
i	*i*th particle
m	metal
p	particle
r	radial
s	solid
w	wall
z	axial

Kalluri et al. [23] studied the effects of microfibrous media on mitigating bed channeling. Yang et al. [24] and Duggirala et al. [25] investigated the effects on external mass transfer in desulfurization by both experiments and CFD modeling. Zhu et al. [26] studied the electrical conductivity of the metal microfibrous sheet in fuel cell. Ryan Sothen [27] discussed MFEC's pressure drop and effective removal of harmful airborne contaminants in air filtration systems.

However, the thermal property of this structure has not been addressed before. Like metal monolith structures, MFEC can be made of highly conductive metals, such as copper, brass, or nickel, to improve the intra-bed heat transfer efficiency in a fixed bed reactor. Such a reactor with conductive metal MFEC may be able to avoid hot or cold spots in the catalyst bed and achieve a uniform temperature profile or fine temperature control. Therefore, there is great potential to apply MFEC for highly exothermic and highly endothermic reactions/processes, especially those having narrow operational temperature windows due to product selectivity requirements and catalyst deactivation issues. To study these applications, the thermal parameters of MFEC are critical and need more research effort to understand them.

The objective of this paper is to give an experimental study of effective thermal conductivity and inside wall heat transfer coefficient for copper, nickel, and stainless steel (SS) MFECs. To understand the improvement of thermal conductivity from sintered fiber structure, a Cu MFEC sample was compared with packed beds (PBs) made of copper and alumina extrudates. Both transient and steady-state measurements were carried out on seven samples. One-phase pseudo-homogeneous approaches were used to analyze radial effective thermal conductivity, axial effective thermal conductivity, and wall heat transfer coefficient for metal MFECs and PBs. Furthermore, Cu MFEC entrapping with 15%Co/Al_2O_3 catalyst particles was employed to study the application of MFEC in FTS reaction. The temperature distribution and product selectivity of Cu MFEC were compared with that of PB catalyst.

2. Materials and methods

2.1. Preparation of MFEC

A wet-lay method to prepare MFEC based on traditional high-speed and low-cost paper-making techniques was developed by Auburn University. The detailed process can be found in Refs. [19–22]. Recently, a new method had been developed by them to prepare the MFEC for pre-manufactured catalyst particles (patent in process [20]), which cannot be applied in metal monolith catalyst structures and metallic foam structures. This new method arises a great potential for MFEC in many heterogeneous catalyst applications with original optimized catalyst recipe, instead of seeking of new recipe for washcoating support. In this study, all metal MFECs were made of 4-μm-diameter and 3-mm-length, and 12-μm-diameter and 3-mm-length metal fibers (IntraMicron, Auburn, AL, USA). After being sintered, the MFEC sheet (Fig. 1) was punched to disks sized to stack into the reactor tube. In order to ensure good contact and avoid dead space between the tube wall and MFEC, the diameter of the MFEC disk was 105% of the ID of the tube.

2.2. Thermal conductivity measurement

As shown in Fig. 2, test materials were loaded in the middle section of a 1.5″ (38.1 mm) OD copper tube, which was immersed in a water bath kept at constant temperature during every measurement. Fine thermocouples (Omega, 1/32″, 0.79 mm) were utilized to measure the temperature profiles of the test materials. For transient tests, as Waddams [29] did, there was no gas passing through the test tube, and the tube was filled with stagnant N_2 at ambient pressure. At $t = 0$, the test apparatus was put into the water bath, where it was heated up from room temperature to the water bath temperature. The heating curve on the midplane was recorded by a data logger (Omega, OM-DAQPRO-5300).

For steady-state tests, a N_2 gas stream at room temperature was fed to the test tube immersed in the water bath and heated up along with the testing materials. The temperature profiles inside the materials were measured after the outlet N_2 stream reached a steady temperature. The locations of the thermocouples are show in Fig. 2.

2.3. Samples for thermal conductivity measurement

Copper, nickel, and SS MFECs entrapping 180- to 250-μm alumina particles (Alfa, pore volume 1.14 cc/g, surface area 245 m^2/g) were prepared for thermal conductivity measurements. Packed beds made of copper powder (Alfa, 180–250 μm, pore volume 0.22 cc/g) and alumina particles of the same size were also evaluated for comparative purposes. The properties of all samples are

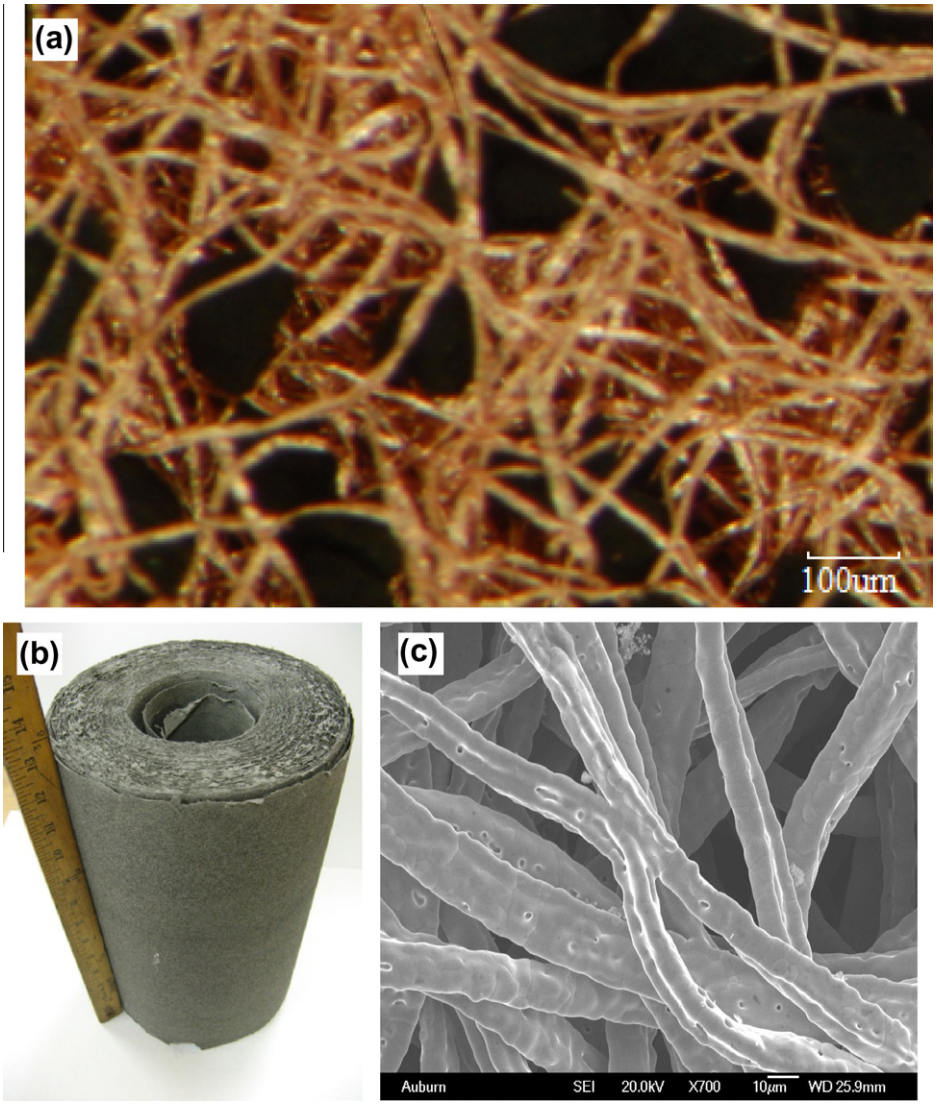

Fig. 1. Pictures of MFECs; (a) 12-μm Cu MFEC with FTS catalyst particles, (b) nickel MFEC roll by paper-making machine, (c) bonding junctions of copper fibers in sample (a).

listed in Table 1. PB 1 consisted of pure copper particles, PB 4 was made of pure alumina particles, and PB 2 and 3 were the mixture of copper and alumina particles. The copper fractions were maintained at such levels that the copper weight fraction of PB 2 and the copper volume fraction of PB 3 were close to these of Cu MFEC.

2.4. FTS experiment

Cobalt nitrate aqueous solution with desired concentration was used to prepare 15 wt.% cobalt metal on 180- to 250-μm alumina particles (surface area, 255 m^2/g; pore volume, 1.14 cc/g; mean pore size, 13.2 nm) by incipient wetness impregnation. The

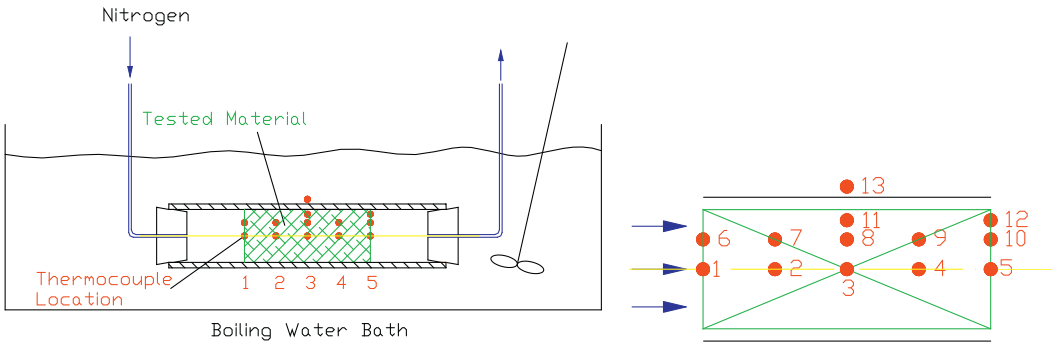

Fig. 2. Apparatus of thermal conductivity measurement (left) and the location of thermocouples (right).

Table 1
Properties of different samples.

		PB 1	PB 2	PB 3	PB 4	Cu MFEC	Ni MFEC	SS MFEC
Volume(%)	Metal[a]	33.59	10.81	8.01	0	7.43	4.9	5.67
	Al_2O_3 [b]	0	45.12	53.99	63.89	29.4	18.16	18.01
	Void	66.41[c]	44.07[c]	38[c]	36.11	63.17	76.94	76.32
Weight (%)	Metal[a]	100	75	65	0	76	77	78
	Al_2O_3	0	25	35	100	24	23	22
Packing density (g/cc)		3.01	1.292	1.1042	0.4363	0.8763	0.5667	0.5821
Volumetric heat capacity (J/cc K)		0.8804	0.5677	0.5500	0.3839	0.3799	0.3084	0.3410

[a] Metal: copper particles in PBs; metal fibers in MFECs.
[b] Pore volume was included.
[c] External void plus internal void of copper powder.

catalyst particles were dried at room temperature overnight and calcined at 648 K with air flowing for 3hr. Then, the calcined catalyst particles were entrapped into a sintered copper fiber matrix to form a Cu MFEC structure (Fig. 1a). Subsequently, circular disks were punched out from MFEC to fit the ID of the FTS reactor, and a small hole was made at the center of the disks to locate the thermocouple at the centerline of the catalyst bed. The disks (5/8 in. in diameter) were 6% bigger in diameter than the reactor tube (15 mm ID), which can offer a good seal at the reactor wall as well as a good contact for a high inside wall heat transfer coefficient. After being loaded into the reactor, the MFEC was reduced in situ at 638 K with hydrogen for 16 h. Then, syngas with H_2/CO ratio 2 and GHSV 5000/h was introduced into the reactor to start up the FTS process. The pressure was set to be 20 bar, and the temperature of reactor wall was adjusted to see the performance of Cu MFEC at different temperature. At the centerline of the catalyst bed, a multipoint thermal couple located, as illustrated in Fig. 3.

In comparison with the Cu MFEC, PB with the same 15 wt.% cobalt on alumina particle was also employed for FTS in the same reactor with the same procedure. According the volume percentage of alumina-supported cobalt catalyst in Cu MEFC, this PB was diluted with flash alumina (180–250 μm) to get the same catalyst density as the Cu MFEC.

2.5. Estimation of the thermal parameters

Transient methods and steady-state methods are widely employed to determine the thermal parameters of porous materials. The transient method based on unsteady radial heat flow was developed by Burke et al. [28] and extended by Waddams [29] by immersing a tube loaded with granulated material in a bath of heated liquid at a uniform temperature while measuring the heating curve on the plane at the middle length of tested material bed. The steady-state method involves flowing fluid through porous materials and recording the temperature profile after reaching a steady state; it is generally used to study the effect of flowing fluid on the thermal parameters of porous material [30,31], which is a realistic situation inside the heterogeneous catalyst reactor. For both methods, it is still challenging to accurately extract the thermal parameters because of the nonlinear relationship between temperature profile and thermal parameters. One-phase pseudo-homogeneous approaches are popular so far, such as one-dimensional models with effective thermal conductivity and wall heat transfer coefficient [32], and two-dimensional models with radial and axial effective thermal conductivity and wall heat transfer coefficient [33]. Two-phase heterogeneous approaches that are much more expensive to calculate are more practical only if the temperature difference between phases is pronounced.

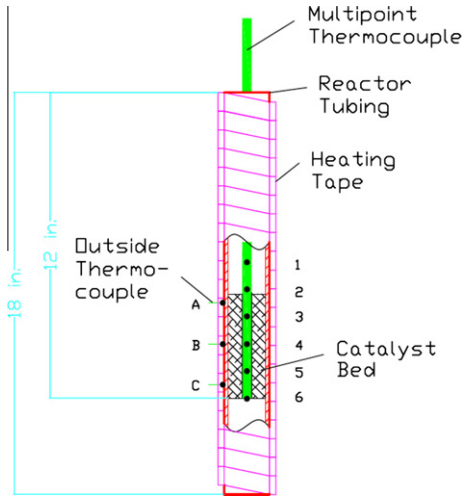

Fig. 3. Sketch of FTS reactor with a multipoint thermocouple at the centerline.

2.5.1. Transient determination

A pseudo-homogeneous one-dimensional model with radial effective thermal conductivity and inside wall heat transfer coefficient was used to analyze this case. The partial differential equation (PDE) describing the heat transfer inside the material is given by

$$\rho(x_m C_{pm} + x_{Al} C_{PAl}) \frac{\partial T}{\partial t} = k_{er} \frac{1}{r} \frac{\partial}{\partial r}\left(r \frac{\partial T}{\partial r}\right) \quad (1)$$

With boundary conditions

$$\frac{\partial T}{\partial r} = 0 \text{ at } r = 0 \quad \text{and} \quad k_{er} \frac{\partial T}{\partial r} = h_w (T_w - T) \text{ at } r = r_w \quad (2)$$

With 40 divisions on radial direction, the PDE describing the transient heat transfer was discretized using a central finite difference scheme and integrated by Euler implicit method [34]. A Newton–Raphson search algorithm was used to determine k_{er} and h_w in

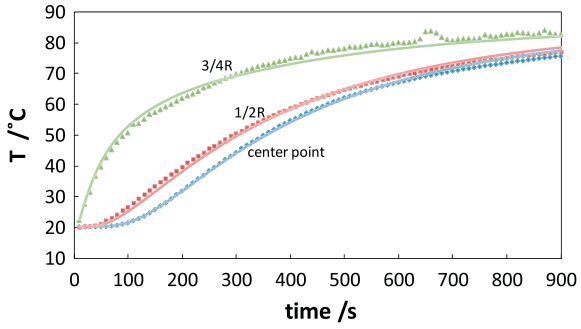

Fig. 4. Temperature–time profile (points) and the numerical fitting result (curves) for PB 3.

the PDE equations by fitting the heating curve from three thermocouples labeled 3, 8, and 11, located at the centerline, $R/2$ and $3R/4$, respectively, on the midplane of the tube. For example, in Fig. 4, the heating curves of sample PB 3 were fitted by the PDE equation with k_{er} 0.182 W/m K and h_w 53.7 W/m^2 K. As a result, this nonlinear regression process provided estimations of the radial effective thermal conductivity, k_{er}, and the inside wall heat transfer coefficient, h_w, for all samples. Standard deviations and standard errors for the parameters corresponding to a 95% confidence interval were estimated by linearized statistics [35].

2.5.2. Steady-state determination

A pseudo-homogeneous two-dimensional model was used to calculate radial and axial effective thermal conductivities and inside wall heat transfer coefficient for the steady-state analysis. All thermocouples shown in Fig. 2 (left) were fitted in this case except points 1 and 6, which were treated as boundary conditions and also initial conditions. The PDE for the heat transfer phenomena inside the media is given by:

$$(\varepsilon\rho_f C_{pf} + (1-\varepsilon)\rho_s C_{Ps})\frac{\partial T}{\partial t} + \rho_f C_{pf} v_z \frac{\partial T}{\partial z} = k_{er}\frac{1}{r}\frac{\partial}{\partial r}\left(r\frac{\partial T}{\partial r}\right) + k_{ez}\frac{\partial^2 T}{\partial z^2} \quad (3)$$

with boundary conditions

$$\frac{\partial T}{\partial r} = 0 \text{ at } r = 0; \quad T = T_1 \quad \text{and} \quad T_6 \text{ at } z = 0 \text{ also } t = 0;$$
$$k_{er}\frac{\partial T}{\partial r} = h_w(T_w - T) \text{ at } r = r_w; \quad \frac{\partial T}{\partial z} = 0 \text{ at } z = L \quad (4)$$

The PDE was discretized using central finite difference formulas and integrated by Euler explicit method [34] from initial condition to steady state. Forty divisions in the radial direction and 20 in the axial direction were employed to mesh the domain. Von Neumann analysis had shown that this scheme was conditionally stable with a courant number smaller than 0.5. The thermal parameters, k_{er}, k_{ez}, and h_w, were determined by fitting the experimental temperature profiles with Newton–Raphson search algorithms. Standard errors of the parameters were estimated using the same method as that in the transient data [35]. For all cases, the standard deviations of k_{er} were smaller than 10%, and the standard deviation of h_w was less than 25%. A higher uncertainty of h_w was observed for low gas flow rate cases due to less data and a smaller temperature gradient.

3. Results and discussion

3.1. Effective thermal conductivity

3.1.1. Transient measurements

For transient tests, the length of the media bed was around 6 in. (152.4 mm), which was four times the tube diameter. According to Waddams [29] and Kozlov [36], the effect of axial heat flow at the midplane can be eliminated because the bed is of adequate length. Thus, the temperature increase in the material at midplane during the transient heat-up process is only from the heat transfer along the radial direction. Therefore, the one-dimensional homogeneous model will be valid for fitting the heating curve on the midplane. The heating curves at center point on the midplane (point 3) of seven samples are presented in Fig. 5. PB 4 and Cu MFEC have close volumetric heat capacities, but the temperature rise of Cu MFEC is much faster than that of PB 4. This suggests that heat transfer in Cu MFEC is much faster than that in an alumina-packed bed, and the effective thermal conductivity and inside wall heat transfer coefficient of Cu MFEC are significantly larger than those of packed beds. This result is confirmed by the nonlinear regression results. As

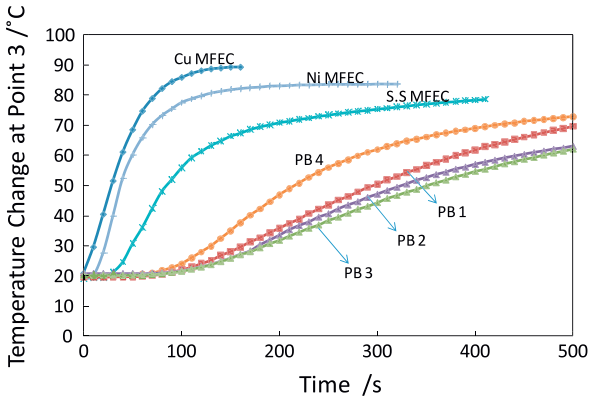

Fig. 5. Temperature–time profiles of center points during transient measurements.

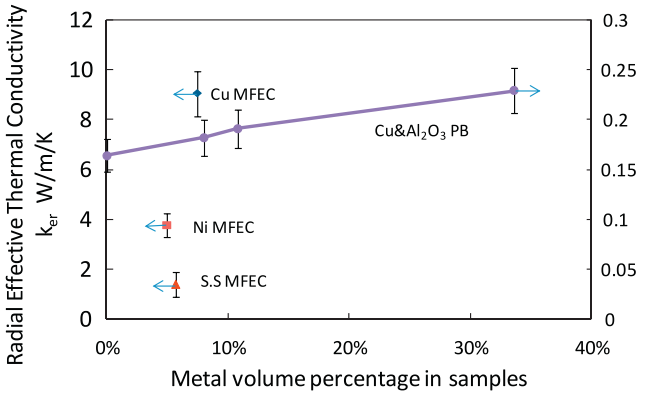

Fig. 6. Radial effective thermal conductivity for MFECs and packed beds extracted from the numerical fitting of transient measurements, standard deviation in 10–15%.

shown in Fig. 6, a MFEC made of copper demonstrates a thermal conductivity of 9.05 W/m K. It is 55 times higher than that of a packed bed made of alumina particles (0.16 W/m K) and 38 times higher than that of pure copper particle bed (0.23 W/m K). In Fig. 7, the inside wall heat transfer coefficient of Cu MFEC (235 W/m^2 K) is 10 times of that of alumina-packed bed (22.7 W/m^2 K) and two times of that of copper particle bed (125 W/m^2 K). MFEC made of SS and nickel also demonstrate high effective thermal conductivities of 1.395 and 3.774 W/m K, respectively. This is the first time that the effective thermal conductivity and wall heat transfer coefficient of MFEC have been determined. Obviously, the

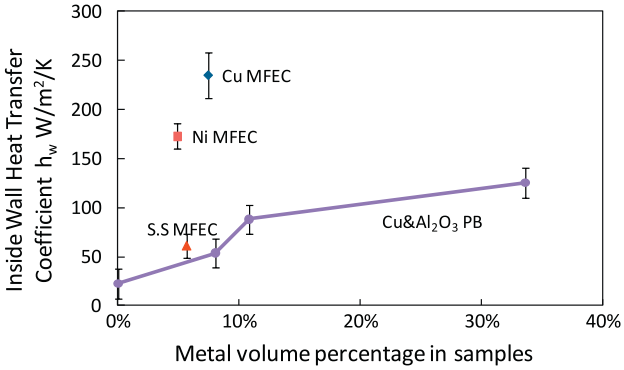

Fig. 7. Inside wall heat transfer coefficient for MFECs and packed beds extracted from the numerical fitting of transient measurements, standard deviation in 15–20%.

effective thermal conductivity of PBs is much lower than that of Cu MFEC, even higher volume percentage of metal for PBs. Therefore, the improvement of thermal conductivity is an effect of a sinter-locked network of metal fibers in MFEC structure, as directly shown in Fig. 1c. This kind of structure provides continuous metal channels or bridges for heat conduction, which are much more effective than the point contacts in powder PBs.

In Figs. 6 and 7, data for PB 1 to 4 are connected as a curve because they are packed beds of various copper particle and alumina particle fractions. The effective thermal conductivities of pure alumina bed (PB 4) and that of pure copper particle bed (PB 1) are consistent with literature data [36–38]. The effective thermal conductivity of the packed beds increases slightly with the copper volume, while all the MFECs demonstrate higher thermal conductivities than any packed bed. However, the inside wall heat transfer coefficient of packed beds rises fast with the copper fraction, which means that the introduction of copper metal greatly improves the heat transfer through the interface between the wall and catalyst bed, while the Cu MFEC still has a higher wall heat transfer coefficient than that of any packed bed. This result suggests that MFEC is superior to metal particle diluted beds in heat transfer. Therefore, metal MFEC efficiently increases thermal conductivity of the catalyst bed, and the combination of high thermal conductivity and high wall heat transfer coefficient is expected to enhance the intra-bed heat transfer for highly exothermic or highly endothermic reactions when the entrapped alumina particle is loaded with precious metals as active catalytic compounds.

3.1.2. Steady-state measurement

For the steady-state thermal conductivity measurement, only 3 in. (76.2 mm) of the test material was loaded in the copper tube. Based on the assumption of homogeneity, thermal parameters, k_{er}, k_{ez}, and h_w, were estimated by fitting the temperature profile. Figs. 8 and 9 give the evolution of radial effective thermal conductivity, k_{er}, of seven samples as different N_2 gas velocities. Here, Re is calculated by

$$Re = \frac{\rho v D_p}{\mu(1-\varepsilon)} \tag{5}$$

where D_p is the equivalent diameter of the sample, given by

$$\frac{1}{D_p} = \frac{S_p}{6V_p} = \sum \frac{y_i}{\varphi_i D_i} \tag{6}$$

Compared with packed beds, the radial effective thermal conductivity of MFEC increases much faster with gas velocity, even with the same volume percent of metal, like in Cu MFEC and PB 3. It is believed that this high thermal conductivity for MFEC is the result of co-enhanced interaction of high conductive contribution from

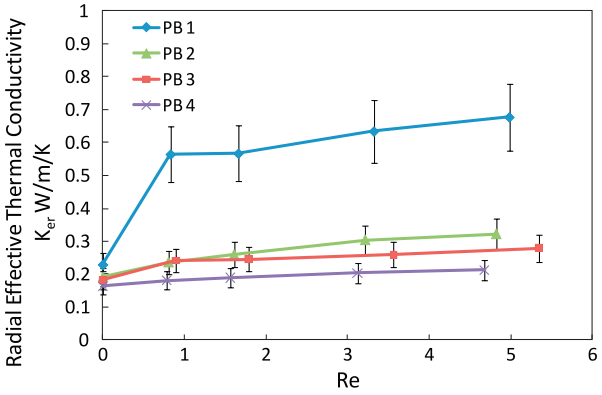

Fig. 9. Radial effective thermal conductivity for packed beds extracted from the numerical fitting of steady-state measurements, standard deviation in 15–20%.

continuous metal channels and high convective contribution from high geometric surface area. Because micron-sized fibers offer large surface area, MFEC has a higher volumetric geometric surface area than packed beds, such as 58,080 m^{-1} for Cu MFEC and 17,670 m^{-1} for alumina PB. This extra geometric surface area of MFEC contributes to the dramatic increase in thermal conductivity, but is not the only reason for it. A poor thermal conductivity term, like for SS MFEC, will limit this trend, producing only have a small gain of thermal conductivity, like the behavior of packed beds. Therefore, the combination of the conduction and convection contributions is accountable for the great increase in radial effective thermal conductivity of MFEC with gas velocity.

Axial thermal conductivity was also determined from the analysis of steady-state measurements. It is determined that the axial thermal conductivity agrees with the equation used by others [39,40].

$$k_{ez} = k_{ez}^0 + 0.5 R_e P_r k_f \tag{7}$$

where k_{ez}^0 is the axial effective thermal conductivity with stagnant gas. For the PBs whose macrostructure is identical in axial and radial direction, k_{ez}^0 is equal to the stagnant radial effective thermal conductivity calculated from the transient measurement. For example, for PB 1, shown in Fig. 10, the intercept of the tendency line, which can be treated as the stagnant axial effective thermal conductivity, is 0.2194 W/m K, which is very close to value of radial effective thermal conductivity from transient test, 0.2291 W/m K. However, the intercepts of MFECs (0.951, 0.773, and 0.663 W/m K) are much lower than the stagnant radial effective thermal conductivity from the transient measurement (9.05, 3.774, and 1.395 W/m K for Cu MFEC, Ni MFEC, SS MFEC, respectively). The

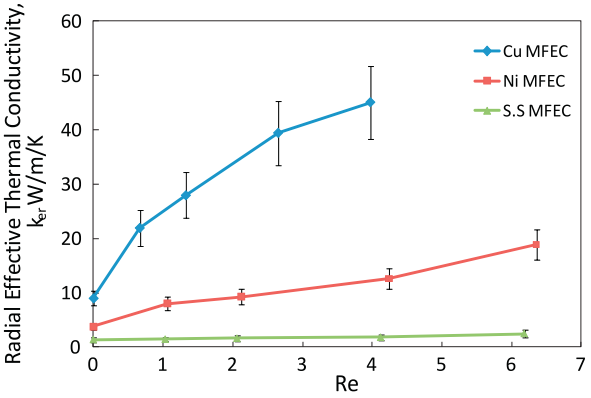

Fig. 8. Radial effective thermal conductivity for MFECs extracted from the numerical fitting of steady-state measurements, standard deviation in 15–20%.

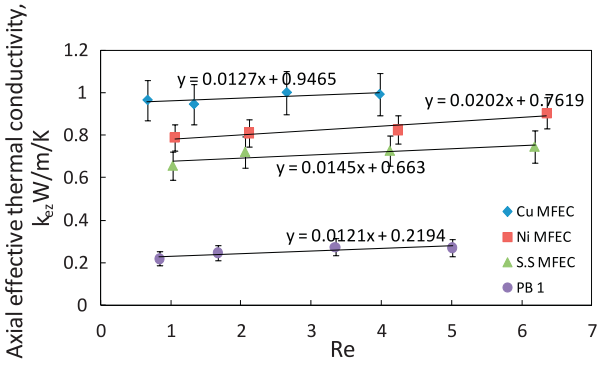

Fig. 10. Axial effective thermal conductivity extracted from the numerical fitting of steady-state measurements, standard deviation in 15–20%.

fiber orientation preference in MFEC prepared by wet-lay manufacture and the separated disks stack loading in the tube can explain this large difference between axial and radial thermal conductivity. During wet-lay manufacture, when water is drained off through the bottom of the hand sheet model and then a metal–cellulose sheet is formed, metal fibers sedimentate freely onto the screen where most of the fibers preferentially lie in the *x*–*y* plane, such that few metal fibers are along the axial direction in MFEC and most fibers prefer an orientation along the radial direction. In addition, the MFEC material is prepared as separated disks with 0.4–2 mm thickness and stacked into the tube one by one. Therefore, MFEC does not offer a continuous metal channel in the axial direction as in the radial direction, which results in radial thermal conductivity of Cu MFEC being nine and one-half times that of the axial thermal conductivity. Because of this direction-dependent thermal property, extra attention is needed for loading the MFEC into the reactor to make use of the high radial thermal conductivity or the high axial thermal resistance.

3.2. Inside wall heat transfer coefficient

The inside wall heat transfer coefficient is also an important thermal parameter for the heat transfer behavior inside the reactor. The temperature difference between the catalyst bed and the wall of the reactor depends on the thermal resistance between them, which is affected by materials and the contact condition. It is noteworthy that the poor inside wall heat transfer is the bottleneck for the application of metal monolith in highly exothermic and highly endothermic reactions [41]. Because the monolith structure is usually prepared with a smaller diameter than the ID of the reactors to easily package inside them, the contact between the monolith and the reactor wall is generally poor, and the inside wall heat transfer coefficient is low. Superior to monolith structure, MFEC, which is much more flexible to be corrugated and shaped, is usually prepared as sheets with a diameter 3–8% bigger than the ID of reactors. Therefore, a good contact between MFEC materials and inside wall of the reactors can be achieved along with a high inside wall heat transfer coefficient.

Although higher uncertainties were shown in the analysis, the result is given in Figs. 7 and 11. Here, the inside wall heat transfer coefficient of MFEC is generally greater than that of PBs. For stagnant conditions, the heat conduction term between the tube wall and the solid phase is the main contributor to the overall wall heat transfer coefficient, which can be improved by introducing a metal like copper into the alumina-packed bed. For gas flowing conditions, the convective heat transfer term becomes more significant; additionally, the wall heat transfer coefficient of all samples increases with gas velocity. With the same metal volume percentage, the heat transfer coefficient of Cu MFEC is obviously higher than that of PB 3. The reason is thought to be that some copper fibers in Cu MFEC are compressed against the wall to provide an edge contact with the tube wall, which is more effective for heat transfer through the interface between MFEC and the wall, while the copper particle bed only has point contacts.

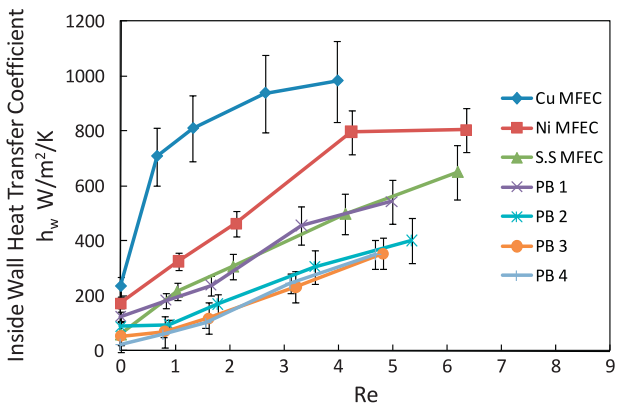

Fig. 11. Inside wall heat transfer coefficient for extracted from the numerical fitting of transient and steady-state measurements, standard deviation in 15–25%.

3.3. FTS result

Copper metal was reported reducing the heavy product selectivity of FTS reaction for the cobalt base catalyst [42]; therefore, the Co/Al_2O_3 catalyst or the Al_2O_3 support needs to be isolated from the paper-making process and sintering of the copper fiber matrix to prevent the copper from contaminating the catalyst. By employing this new method to load the pre-manufactured catalyst particles, calcined Co/Al_2O_3 particles were combined with pre-sintered copper fiber matrix to form Cu MFEC structures. The advantages of this method are not only that the washcoating process required in monolith and metallic foams could be eliminated, but also that the decomposition of copper on the surface of Al_2O_3 support during the preparations of MFEC can be reduced to keep the original surface chemistry composition of the entrapped catalyst, along with the activity and the selectivity. Furthermore, intra-particle mass transfer was enhanced due to the small particle size used in this material versus typical extrudates used in industrial fixed bed reactors. Hence, a fast reaction rate was maintained in the catalyst bed, which requires an enhanced heat transfer catalyst structure like MFEC to remove the reaction heat from catalyst bed to cooling surface.

In the FTS process, without the gas/liquid recycle, the gas superficial velocity is usually small because of the high pressure (superficial velocity for our test is 0.92 mm/s), so that the convective contribution of the heat transfer is minimized. Additionally, at the beginning of the catalyst bed, which generally is the highest reaction rate zone, as well as the highest reaction heat generation section, the liquid product is small, so that the conduction from liquid is also limited. Therefore, for FTS, a catalyst structure with an enhanced heat transfer characteristics from the self-dependent conduction is desired. For PB, the effective thermal conductivity of alumina particle is only 0.16 W/m K in stagnant N_2 gas. Even the corrugated packing is reported to have an effective radial thermal conductivity between 1 and 2 W/m K [16]. In contrast, for copper MFEC, the effective thermal conductivity is around 9.05 W/m K, which is expected to achieve much improvement of the intra-bed heat transfer inside the catalyst bed from the standard packed bed structure.

FTS reaction with PB and copper MFEC was carried out at different temperatures, each temperature running for 1 day with the order listed in Table 2. For the same conversion of the FTS test, the reaction heat was same, but the temperature difference from centerline to reactor wall was much lower for Cu MFEC. When the conversion increased with higher wall temperature, more reaction heat was produced inside the catalyst bed, which made the temperature difference rise again. For PB, the temperature difference grew much faster than that of copper MFEC. It gained 70.2 °C difference at 255 °C wall temperature for this 15-mm ID reactor, and a runaway state was already reached where the methanation reactions dominated (Fig. 12). Because of poorly heat transfer characteristics of PB that produces a higher temperature profile inside the catalyst bed, the cobalt-time-yield was higher for PB than that for Cu MFEC at the same wall temperature from day 1 to day 4. It is notable that the runaway state of PB caused a quick deactivation of the catalyst, cobalt-time-yield declined to 1/3 from day 2 to day 5, probably because of the high temperature sintering or carbon deposition during runaway on day 4. The application of copper

Table 2
Temperature and selectivity of FTS test with two types of catalysts at 20 bar, H2/CO ratio 2 and 5000/h GHSV.

Day	T_{wall} (°C)	Highest centerline T (°C)		Conversion	Cobalt-time-yield 10^{-3} (mol_CO/mol_cobalt/s)	Selectivity	
		T	$T - T_{wall}$			α value	C_{5+}
PB, Co/Al_2O_3, diluted with fresh Al_2O_3							
1	225	230.7	5.7	0.357	3.32	0.834	0.797
2	235	243.1	8.1	0.534	4.96	0.819	0.734
3	245	259.7	14.7	0.87	8.09	0.725	0.506
4	255	325.2	70.2	1	9.29	0.151[a]	0.124
5	235	237.1	2.1	0.183	1.70	0.822	0.753
Cu MFEC, entrapping Co/Al_2O_3, 7.4 vol%Cu, 29 vol%Al_2O_3							
1	225	224.6	−0.4	0.151	1.40	0.852	0.821
2	235	237.8	2.8	0.387	3.62	0.831	0.793
3	245	250	5	0.516	4.80	0.815	0.738
4	255	264.4	9.4	0.789	7.33	0.797	0.702
5	235	237.6	2.6	0.371	3.45	0.836	0.801

[a] Runaway, α value based on methane selectivity.

MFEC can avoid runaways at relative high temperature, so that a much even temperature profile can be maintained inside the catalyst bed and low deactivation can be achieved. Without fatally damaging the catalyst and sharply decreasing the product, copper MFEC provides a larger operation temperature range and better control.

The chain growth probability factor (α) of FTS is dependent on the catalyst temperature, with high temperature giving a low α value. Due to the higher effective thermal conductivity of copper MFEC, the intra-bed heat transfer was greatly enhanced and a more uniform temperature distribution inside the catalyst was achieved. The α value also was improved by MFEC structure, as shown in Fig. 12. Because higher thermal conductivity promises a smaller temperature difference so that the actual catalyst temperature was much lower for copper MFEC than that for PB, the improvement of α value was much significant for high wall temperature or for large diameter reactors which also have high centerline temperature. This confirmed the temperature difference between centerline and reactor wall, which was higher for high wall temperature. Therefore, the application of copper MFEC gave a higher α value and desired heavier product selectivity, like C_{5+}. Although copper is a catalyst for methanol synthesis, the surface area of copper fiber is only 0.7% of the total surface area of alumina, so that methanol synthesis is negligible in MFEC with Co/Al_2O_3, which was proved by the FTS product analysis, only 15 ppm methanol in water phase.

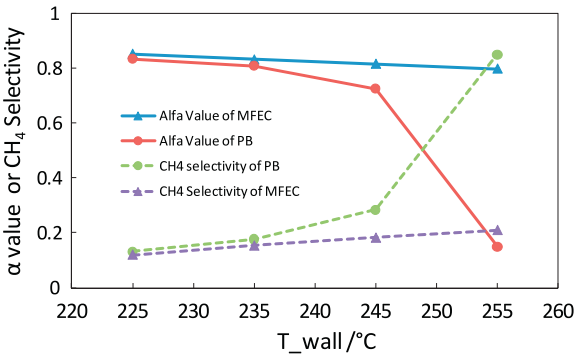

Fig. 12. The chain growth probability factor vs. reactor wall temperature for PB and Cu MFEC.

4. Conclusions

The enhanced heat transfer characteristic of Cu, Ni, and stainless steel MFEC was studied by experimental determination of thermal parameters, along with those of PBs made of copper powder or alumina particles or mixtures. In stagnant N_2 gas test, Cu MFEC demonstrated 56 times higher radial effective thermal conductivity, 9.05 W/m K, and more than 10 times higher inside the wall heat transfer coefficient, 235 W/m^2 K, than a traditional alumina-packed bed. Nickel and SS MFEC also demonstrate high effective thermal conductivities of 3.774 and 1.395 W/m K, respectively. With the same volumetric loading of copper, or even higher in PB, the radial effective thermal conductivity of Cu MFEC is much greater than that of PB, because the metal fibers forming sinter-locked network in MFEC structure provide continuous metal channels or bridges for heat conduction, which are much more effective than the point contacts in powder PBs. Because of this high thermal conductivity dependent on self-structure, MFEC can provide enhanced heat transfer for highly exothermic or highly endothermic reactions, even without recycle of gas or liquid to increase the convective contribution, which is generally required in corrugated packing.

With gas passing through the tested materials, the MFEC structure offers more volumetric geometric surface area for the convective contribution of heat transfer than the structure of PB, which further increases the effective thermal conductivity of MFEC. However, due to the fiber orientation preference in MFEC structure and the separated disk's stack loading in the tube, the axial effective thermal conductivity is much lower than the radial effective thermal conductivity. The stagnant axial effective thermal conductivity of Cu MFEC is 0.951 W/m K, only 1/9.5 of the radial effective thermal conductivity. Furthermore, the inside wall heat transfer coefficient is also improved by the MFEC structure because MFEC introduces metal into catalyst bed and some fibers are bent by compressive forces to provide an edge contact with the tube wall.

In the FTS tests, the pre-manufactured FTS catalyst particles were entrapped into sintered Cu fiber matrices to form Cu MFEC structure. Cu MFEC demonstrated an enhanced intra-bed heat transfer property, which caused a much more uniform temperature distribution through the catalyst bed. The application of Cu MFEC in FTS demonstrated that the hat spot and runaway could be effective prevented at high temperature, and higher reaction activity and higher hydrocarbon product selectivity were maintained. Furthermore, intra-particle mass transfer was enhanced due to the presence of small particles in this material versus typical extrudates used in industrial fixed bed reactors. In summary, compared to a typical PB structure, Cu MFEC offers a larger operation temperature range or bigger size reactors for FTS with better product selectivity.

For highly exothermic or highly endothermic reactions, conductive metal MFEC, especially Cu MFEC, rises a high effective thermal conductivity for the catalyst bed to enhanced intra-bed heat transfer as conductive monolith structure or other enhanced heat transfer catalyst structures. However, the compatibility of pre-manufactured catalyst particles and high self-dependent thermal conductivity, flexibility, and ease to be corrugated and additionally shaped make the MFEC structure a lot of applications in heterogeneous reaction. For instance, the MFEC structure is also a good candidate for the packing material of reactive distillation, on the subject of which requires more research.

Acknowledgments

This work was supported by US Navy under a US Navy contract at Auburn University (N00014-09-C-0208) administered through

the Office of Naval Research. The authors want to thank IntraMicron (Auburn, AL, US) for technical support.

References

[1] H. Kölbel, M. Ralek, Catal. Rev. – Sci. Eng. 21 (1980) 255–274.
[2] S.T. Sie, R. Krishna, Appl. Catal. A 186 (1999) 55–70.
[3] D.S. Van Vuuren, CSIR CENG (1982) 432.
[4] D.J. Duvenhage, T. Singles, Catal. Today 71 (2002) 301–305.
[5] S. Groueff, Manhattan Project: The Untold Story of the Making of the Atomic Bomb, Little, Brown and Co., Boston, 1967.
[6] R.L. Espinoza, A.P. Steynberg, B. Jager, A.C. Vosloo, Appl. Catal. A 186 (1999) 13–26.
[7] R. Krishna, S.T. Sie, Fuel Process. Technol. 64 (2000) 73–105.
[8] A.M. Hilmen, E. Bergene, O.A. Lindvag, D. Schanke, S. Eri, A. Holmen, Catal. Today 69 (2001) 227–232.
[9] R.M. Deugd, F. Kapteijin, J.A. Moulijin, Catal. Today 79 (2003) 495–501.
[10] K. Pangarkar, T.J. Schildhauer, et al., Ind. Eng. Chem. Res. 47 (2008) 3720–3751.
[11] K. Pangarkar, T.J. Schildhauer, et al., Catal. Today 147s (2009) s2–s9.
[12] A.P. Steynberg, M.E. Dry, Fischer–Tropsch Technology, Elsevier Science & Technology Books, 2004.
[13] E. Tronconi, G. Groppi, T. Boger, A. Heibel, Chem. Eng. Sci. 59 (2004) 4941–4949.
[14] C.G. Visconti, E. Tronconi, et al., Appl. Catal. A 370 (2009) 93–101.
[15] L. Giani, G. Groppi, E. Tronconi, Ind. Eng. Chem. Res. 44 (2005) 4993–5002.
[16] C. von Scala, M. Wehrli, G. Gaiser, Chem. Eng. Sci. 54 (1999) 1375–1381.
[17] B.J. Tatarchuk, M.F. Rose, A. Krishnagopalan, J.N. Zabasajjia, D. Kohler, US Patent 5096,663, March 17, 1992.
[18] B.J. Tatarchuk, M.F. Rose, A. Krishnagopalan, J.N. Zabasajjia, D. Kohler, US Patent 5304,330, April 19, 1994.
[19] L.L. Murrell, F.M. Dautzenberg, R.A. Overbeek, B.J. Tatarchuk, US Patent 20020068026, June 6, 2002.
[20] B.J. Tatarchuk, H. Yang, R. Kalluri, D.R. Cahela, US Patent, Provisional No. 12/940792.
[21] M.W. Meffert, Ph.D. dissertation, College of Engineering, Auburn University, Auburn, AL, 1998.
[22] R.K. Duggirala, Ph.D. dissertation, College of Engineering, Auburn University, Auburn, AL, 2008.
[23] R.R. Kalluri, D.R. Cahela, B.J. Tatarchuk, Sep. Purif. Technol. 62 (2008) 304–316.
[24] Hongyun Yang, D.R. Cahela, B.J. Tatarchuk, Chem. Eng. Sci. 63 (2008) 2707–2716.
[25] R.K. Duggirala, C.J. Roy, H.Y. Yang, R.R. Kalluri, D.R. Cahela, B.J. Tatarchuk, 232nd ACS National Meeting, September 2006, San Francisco, CA, USA.
[26] Wenhua H. Zhu, M.E. Flanzer, B.J. Tatarchuk, J. Power Sources 112 (2002) 353–366.
[27] Ryan Sothen, Ph.D. dissertation, College of Engineering, Auburn University, Auburn, AL, 2009.
[28] S.P. Burke, T.E. Schuman, V.F. Parry, Fuel 10 (1931) 249.
[29] A.L. Waddams, J. Soc. Chem. Ind. 63 (1944) 337–340.
[30] A.P. Collier, A.N. Hayhurst, et al., Chem. Eng. Sci. 59 (2004) 4613–4620.
[31] O. Laguerre, S.B. Amara, D. Flick, Appl. Therm. Eng. 26 (2006) 1951–1960.
[32] J.G.H. Borkink, K.R. Westerterp, AIChE J. 38 (1992) 703–715.
[33] M.F.P. Moreira, M.C. Ferreira, J.T. Freire, Chem. Eng. Sci. 61 (2006) 2056–2068.
[34] John D. Anderson, Computational Fluid Dynamics the Basics with Applications, McGraw Hill, 1995.
[35] A. Bjorck, Numerical Methods for Least Squares Problems, SIAM, 1996.
[36] V.A. Kozlov, V.V. Toporova, Powder Metall. Met. Ceram. V12 (1973) 9–12.
[37] R.A. Mischke, J.M. Smith, Ind. Eng. Chem. Fundam. 1 (1962) 288–292.
[38] Kanan Bala, Pradeep R. Pradhan, J. Phys. D: Appl. Phys. 22 (1989) 1068–1072.
[39] A.G. Dixon, J.H. Dongeren, Chem. Eng. Process 37 (1998) 23–32.
[40] D. Wen, Y. Ding, Chem. Eng. Sci. 61 (2006) 3532–3542.
[41] T. Boger, A.K. Herbel, Chem. Eng. Sci. 60 (2005) 1823–1835.
[42] G. Jacobs, M.C. Ribeiro, et al., Appl. Catal. A 361 (2009) 137–151.